Chemical Physics 482 (2017) 192–200

Contents lists available at ScienceDirect

Chemical Physics

journal homepage: www.elsevier.com/locate/chemphys

Electron transfer mediated decay in NeXe triggered by K-LL Auger decay of Ne

Vasili Stumpf [a], Simona Scheit [a], Přemysl Kolorenč [b], Kirill Gokhberg [a,*]

[a] Theoretische Chemie, Physikalisch-Chemisches Institut, Universität Heidelberg, Im Neuenheimer Feld 229, D-69120 Heidelberg, Germany
[b] Charles University in Prague, Faculty of Mathematics and Physics, Institute of Theoretical Physics, V Holešovičkách 2, 180 00 Prague, Czech Republic

ARTICLE INFO

Article history:
Available online 24 August 2016

ABSTRACT

In this article we present the results of an *ab initio* study of electron transfer mediated decay (ETMD) in NeXe dimer triggered by the K-LL Auger decay of Ne. We found that the $Ne^{2+}(2p^{-2}\ ^1D)Xe$ and $Ne^{2+}(2p^{-2}\ ^1S)Xe$ states which are strongly populated in the Auger process may decay by ETMD emitting a slow electron and leading to the Coulomb explosion of the dimer which results in Ne^+ and Xe^{2+} ions. We also computed the corresponding decay widths, the ETMD electron spectra, and the kinetic energy release of the nuclei (KER) spectra. We showed that the spectra corresponding to the decaying states which derive from the two multiplets have completely different shape which reflects differing accessibility of the ETMD final states. Thus, in the $Ne^{2+}(2p^{-2}\ ^1S)Xe$ state ETMD is allowed for all interatomic distances accessible in nuclear dynamics, while in the $Ne^{2+}(2p^{-2}\ ^1D)Xe$ state the ETMD channels become closed one by one. This in turn leads to the different behavior of the ETMD decay widths and ultimately the spectra. We show how these differences make it possible to study ETMD of the two states separately in a coincident measurement. We also discuss how the dynamics which follow ETMD in the final state manifold may lead to the appearance of the unusual products: Ne, Xe^{3+} and a slow electron.

1. Introduction

The initial effect of ionizing radiation interacting with a weakly bound medium is to ionize or excite constituent atoms and molecules. The energy invested locally by photon absorption dissipates through a sequence of relaxation processes, with the processes involving electronic degrees of freedom being among the fastest. For highly excited electronic states local autoionization processes such as Auger decay [1] take place. However, in a medium ultrafast electronic decay may occur even if the local autoionization channels are closed. As Cederbaum and co-workers showed in 1997 [2], inner-valence vacancies in small hydrogen-bonded clusters of HF which cannot decay in the Auger process decay instead in the process they named interatomic Coulombic decay (ICD). In ICD the excess energy on the monomer with the inner-valence hole is transferred to a neighbor ionizing it. Numerous investigations published since the original article have established, first, that the process is completely general and occurs for any type of electronic excitation which has sufficient energy to ionize its environment [3]. Second, that it occurs on the femtosecond timescale [3] and is efficient in quenching concurrent processes such as photon emission [4] or molecular dissociation [5,6]. Third, that ICD is an integral part of complex de-excitation cascades which follow ionization or excitation of deeply lying core levels [7–10]. Efficient ionization of the environment, such as solvent, inherent in ICD, as well as production of electrons in the range of few to a few tens of eV make this process important in explaining radiation damage to molecules [11].

To a large extent the success in studying the properties of ICD can be attributed to close collaboration among theorists and experimentalists. This collaboration has been particularly fruitful in investigating ICD in rare gas dimers where both *ab initio* calculations and the experimental observations can be done with a great degree of detalization and to high precision. Thus, the theoretical investigation of ICD in Ne dimer [12,13] was a motivation for the first unambiguous experimental observation of ICD [14] which, in turn, led to refined calculations [15] to account for the discrepancies between the experimental and the previous theoretical results. This call-and-response interaction between the experiment and theory and the reliance on rare gas dimers to clarify the fundamental properties of ICD have led to its successful investigation as part of Auger driven cascades [7,8,16–18], in extreme quantum systems such as He dimer [19], or as it progresses in real time [20,21].

Contrasted with the success of studying ICD the theoretical and experimental investigation of a related interatomic

* Corresponding author.
E-mail address: kirill.gokhberg@pci.uni-heidelberg.de (K. Gokhberg).

http://dx.doi.org/10.1016/j.chemphys.2016.08.018
0301-0104/

process – electron transfer mediated decay (ETMD) – lags behind. The process was originally demonstrated by Zobeley et al. to occur together with ICD in mixed rare gas clusters following the inner-valence ionization of constituent atoms [22]. In ETMD a neighbor donates an electron to an ionized species and the released energy is used to ionize the donor (ETMD(2)) or another neighbor (ETMD(3)). The ETMD is possible whenever the electron attachment energy of an ion is larger than the double ionization potential of its environment. Both the original publication and the subsequent theoretical work [23] have shown that for inner-valence ionized systems the rate of ETMD (picosecond timescale) is orders of magnitude smaller than the one of ICD making it a minor decay channel.

However, should ICD become energetically forbidden, ETMD may become the leading relaxation process. *Ab initio* calculations helped to identify a number of mixed small rare gas clusters where the ICD channel for the inner-valence ionized state is either outright forbidden ($ArKr_2$, $KrXe_2$) [24,25] or is allowed for geometries which the cluster cannot access ($ArXe_2$) [26]. Even if ICD becomes allowed in larger clusters such as Ar_mXe_n it does not occur with the nearest neighbors and its rate becomes comparable to that of ETMD [27]. First unambiguous experimental observation of ETMD was achieved simultaneously in larger Ar_mKr_n clusters following the 3s-ionization Ar [28], and in Ar_2 after the double Auger decay of the 2p-vacancy which populates the states in which ICD is either forbidden or slow [29].

It has been only recently realized that multiply, or even singly, ionized atoms with holes in the outer-valence shells represent a general type of a system where ETMD is the leading electronic decay process when such ions are embedded in a suitable environment [30,31]. Such electronic states carry little or no excess energy in isolated ions, therefore, ICD channels are closed in a medium. On the other hand their electron attachment energy is often larger than the double ionization potential of the neighboring species enabling ETMD.

The multiply charged ions are produced in abundance following the Auger decay process, and the subsequent ETMD step leads to their partial neutralization, while the neighbors become doubly ionized and a slow electron is set free. This ETMD driven neutralization has been demonstrated theoretically in $NeKr_2$ clusters, where it was shown to occur within a few picoseconds at the equilibrium geometry of the cluster and to be considerably accelerated due to the motion of the nuclei [30]. ETMD leading to the rapid neutralization of multiply charged species was found to be a crucial step in the de-excitation cascades initiated by X-ray photoabsorption of the microsolvated metal ions [32] where it occurs already within a few tens of femtoseconds. The ETMD of the outer-valence ionized states is also an efficient way of producing doubly ionized species in a medium. Thus, the ETMD driven single-photon double ionization was theoretically shown to be the leading ionization mechanism for atoms and molecules embedded in He environment [31]. This process has been recently experimentally demonstrated in He nanodroplets doped with the Mg_n clusters [33].

For all the investigations of ETMD reported so far no study analogous to the exemplary work on ICD in Ne_2 has been carried out. In this article we discuss a rare gas dimer which can be used for a detailed investigation of ETMD both *ab initio* and experimentally. We present here the results of calculations of the ETMD process in the NeXe dimer which takes place following the normal Auger decay of a 1s-vacancy in Ne. The latter process leads predominantly to the production of the $Ne^{2+}(2p^{-2})$ ions (≈70%) which continue decaying in the ETMD(2) process with Xe. This leads in turn to the emission of a slow electron and the production of Ne^+ and Xe^{2+} ions which fly apart in a Coulomb explosion as is shown by the following equation

$$\begin{aligned} Ne^{2+}(2p^{-2})Xe &\rightarrow Ne^{+}(2p^{-1})Xe^{2+}(5p^{-2}) + e_{ETMD} \\ &\rightarrow Ne^{+} + Xe^{2+} + e_{ETMD}. \end{aligned} \quad (1)$$

The proposed system is the only rare-gas dimer where ETMD of the outer-valence ionized atom can be observed in an electron–ion–ion coincidence experiment following a one step Auger process [34]. This system has important advantages over higher charged states necessary in other dimers (see the Ar_2 case in Ref. [29]). First, the doubly ionized states are more tractable computationally than the higher charged states. Second, they are efficiently produced in the one-step Auger decay, while to obtain higher charged states one needs to rely either on the double Auger process with its relatively low yields or on complicated Auger decay cascades. In what follows we present the results of an *ab initio* computation of the energies and the ETMD rates of the $Ne^{2+}(2p^{-2})Xe$ states, as well as the experimentally observable ETMD electron and nuclear kinetic energy release spectra.

2. Computational methods

2.1. Potential energy curves

The NeXe ground state potential energy curve (PEC) was computed by the coupled cluster singles, doubles and perturbative triples (CCSD(T)) method implemented in the GAMESS-US 2011 quantum chemistry package [35]. For this purpose we used the aug-cc-pVQZ basis set on neon and the aug-cc-pVQZ-PP basis set on xenon, taking the scalar relativistic effects on xenon into account by a 28-electron effective core potential [36]. An additional mid-bond basis set containing 3 *s*-type, 3 *p*-type, 2 *d*-type, 2 *f*-type, 1 *g*-type (3*s*3*p*2*d*2*f*1*g*) basis functions was used to improve the description of the electronic density between the atoms [37]. The resulting curve was corrected for the basis set superposition error.

The potential energy curves for the *doubly* ionized decaying states and the *triply* ionized ETMD final states in NeXe were obtained by adding the corresponding non-relativistic ionization energies to the energy of the NeXe electronic ground state. The double and triple ionization energies were in turn computed within the framework of the Algebraic Diagrammatic Construction (ADC) scheme based on the perturbational expansion of the two-particle and three-particle propagator, respectively, complete up to second order in perturbation theory (ADC(2)) [38,39]. The double ionization energies were computed using the strict version of the ADC (2) method in which there is no coupling within the 3-hole-1-particle block. The extended version of the ADC(2) scheme, where the coupling within the 4-hole-1-particle block is taken to first order, was used to compute the triple ionization energies. The calculation of the respective ionization energies also allows to determine which electronic decay channels are open for each specific decaying state; this information is important for the calculation of the total and partial decay widths described below.

The relativistic effects are important in the final triply ionized Ne^+Xe^{2+} and $NeXe^{3+}$ states accessible via ETMD. The most prominent of them – the spin–orbit splitting of the $Ne^+(2p^{-1}\,{}^2P)Xe^{2+}(5p^{-2}\,{}^3P)$ state – is taken into account phenomenologically. Obtaining the ETMD final state manifold which comprises the correct interactions between Ne^+Xe^{2+} and $NeXe^{3+}$ states requires full relativistic calculations. They were not done, since as we discuss below the phenomenological model derived from the non-relativistic results leads to the ETMD spectra of sufficient accuracy. Moreover, the relevant electronic decay widths can be currently computed only non-relativistically, making the utility of fully relativistic PECs questionable.

The NeXe reference electronic state, molecular orbitals and electron integrals required by the ADC calculations were computed by the restricted Hartree–Fock method as implemented in the MOLCAS 7.4 package [40]. We used cc-pVQZ basis set on neon and the nonrelativistic cc-pVQZ basis by Mahler et al. [41] in the ionization energies' calculations.

2.2. Electronic decay widths

The ETMD widths were calculated by means of the Fano–ADC–Stieltjes method [23,42,43]. According to the Fano approach [44] the total decay width, Γ, can be found from the coupling term between the bound part $|\Phi_b\rangle$ of the resonance wave function and its continuum part at the corresponding resonance energy, $|\chi_{f,\epsilon}\rangle$:

$$\Gamma = 2\pi\sum_f |\langle\Phi_b H_{el}\chi_{f,\epsilon}\rangle|^2, \tag{2}$$

where H_{el} denotes the electronic Hamiltonian and f enumerates open decay channels. The bound and continuum parts of the resonance wave function as well as the coupling between them were constructed by means of the extended second order adiabatic diagrammatic construction (ADC(2)x) scheme for the two-particle propagator [42].Within this scheme the many-electron wave functions are expanded in the intermediate state basis $\tilde{\Psi}_I^{N-2}$ (see Ref. [45]) which spans the $2h$ (two-hole) and $3h1p$ (three-hole one-particle) space built on top of a reference function [38]. In the particular case of the ADC(2)x method the spin-adapted $3h1p$ intermediate states $\tilde{\Psi}_I$ are just the corresponding $3h1p$ configuration state functions which are obtained by the application of the physical excitation operators C_I to the restricted Hartree–Fock ground state $|\Phi_0\rangle$

$$\tilde{\Psi}_I^{N-2} = C_I|\Phi_0\rangle = c_p^\dagger c_k c_l c_m|\Phi_0\rangle, \tag{3}$$

where c_k, c_l, c_m denote the annihilation operators acting on occupied orbitals and $c_p^\dagger$ the creation operator acting on virtual orbitals.

The bound and continuum components of the resonance wave function are obtained by diagonalizing the projections of the ADC Hamiltonian matrix onto the $\mathcal{Q}$ (initial) and $\mathcal{P} = 1 - \mathcal{Q}$ (final) subspaces, respectively. The final subspace comprises all open channels whose total number, n_{open}, and electronic structure are ascertained in the calculation of the triply ionized states described in the previous section. To construct the $\mathcal{P}$-subspace we first note that the $3h1p$ configurations in Eq. (3) represent the final triply ionized states with a continuum electron remaining in the vicinity of the system. Holding the particle index p constant and varying the hole indices we select a subset of intermediate states. This subset is used to construct and diagonalize a Hamiltonian matrix which yields the *adapted* [43] states

$$|\Theta_J^{(p)}\rangle = \sum_I c_{IJ}|\tilde{\Psi}_I^{N-2}\rangle. \tag{4}$$

The spectrum of these states usually has a similar structure to the spectrum of triply ionized states which allows one to identify different channels. Thus, the lowest n_{open} adapted states are taken to represent the open decay channels and are added to the $\mathcal{P}$ subspace, while the rest is added to the $\mathcal{Q}$ subspace. This procedure is repeated for all p's producing the $\mathcal{P}$ subspace. To obtain the complete $\mathcal{Q}$ subspace one should augment the corresponding set of the adapted states by adding to it all $2h$ intermediate states.

In NeXe ETMD proceeds predominantly into the states of the $Ne^+(2p^{-1})Xe^{2+}(5p^{-2})$ character. There are 90 different $Ne^+(2p^{-1}\ ^2P)Xe^{2+}(5p^{-2})$ non-relativistic final states which split into three groups derived from the ^3P, ^1D and ^1S multiplets of $Xe^{2+}(5p^{-2})$. The spin multiplicity of the final states when a continuum electron is added can be either 2 or 4. The spin-quartet states are inaccessible in the electronic decay, since the decaying states in our system are spin-singlet and the coupling term is spin free. This leaves 27 doubly degenerate spin-doublet Ne^+Xe^{2+} final states accessible at large interatomic distances, and we chose the corresponding number of adapted states to represent the $\mathcal{P}$ subspace. At intermediate interatomic distances, where the decay into the $Ne^+Xe^{2+}(5p^{-2}\ ^1S)$ states is forbidden, only 24 adapted states are used to construct $\mathcal{P}$, while the 3 adapted states lying just above them are removed from the calculation. At short interatomic distances, where only the channels corresponding to $Ne^+Xe^{2+}(5p^{-2}\ ^3P)$ are open, the $\mathcal{P}$ subspace contains only the lowest 9 adapted states. It has to be remarked that the states removed from the $\mathcal{P}$ subspace when the corresponding channels are closed do not enter the $\mathcal{Q}$ subspace to avoid irregular behavior of the decay width with the interatomic distance.

Diagonalizing the electronic Hamiltonian projected onto the $\mathcal{Q}$ subspace, $\mathcal{Q}H_{el}\mathcal{Q}$, one obtains the decaying states $|\Phi_b\rangle$ and the corresponding energies E_b which can be taken with sufficient accuracy as the positions of the respective resonances. The diagonalization of the $\mathcal{P}H_{el}\mathcal{P}$ projection of the electronic Hamiltonian yields the discrete pseudocontinuum states $\tilde{\chi}_r$, having the energies $\tilde{E}_r$

$$\tilde{E}_r = \langle\tilde{\chi}_r|PH_{el}P|\tilde{\chi}_r\rangle \tag{5}$$

and coupled to the decaying state $|\Phi_b\rangle$ via the $\mathcal{P}H_{el}\mathcal{Q}$ part of the Hamiltonian. The pseudocontinuum states obtained in an L^2 calculation have wrong normalization and asymptotic behavior. However, we obtain accurate value and the correct dimensionality of the decay width Γ by applying the Stieltjes imaging procedure [46,42] to the auxiliary quantities

$$\tilde{\gamma}_r = 2\pi|\langle\Phi_b|QH_{el}P|\tilde{\chi}_r\rangle|^2. \tag{6}$$

The procedure described above is used to compute the total ETMD width of $Ne^{2+}(2p^{-2})Xe$ states. The partial ETMD widths, Γ_f, corresponding to the decay into the specific $Ne^+(2p^{-1})Xe^{2+}(5p^{-2})$ states correlating with different multiplets of Xe^{2+} were computed by the projection operator approach described in Ref. [23] for the $Ne^{2+}(2p^{-2}\ ^1D)Xe$ decaying states. Similar computation was not possible in the case of the $Ne^{2+}(2p^{-2}\ ^1S)Xe$ decaying state due to the strong mixing of the $Ne^+(2p^{-1})Xe^{2+}(5p^{-2})$ and $NeXe^{3+}(5p^{-3})$ final states.

Within this approach the total final subspace is represented as

$$\mathcal{P} = \sum_f \mathcal{P}_f \tag{7}$$

where $\mathcal{P}_f$ is a projector on the channel f. The partial widths are obtained from the auxiliary quantities

$$\tilde{\gamma}_r^{(f)} = 2\pi|\langle\Phi_b|QH_{el}P_f|\tilde{\chi}_r\rangle|^2. \tag{8}$$

similarly to the case of the total width. In constructing the projector operators P_f we relied on the fact that the intermediate states spanning the subspace $\mathcal{P}$ are just the $3h1p$ configuration state functions (see Eq. (3)). Thus, a Hamiltonian matrix is built within the basis of $3h$ configurations

$$|\Phi_L^{N-3}\rangle = C_L|\Phi_0\rangle = c_k c_l c_m|\Phi_0\rangle, \tag{9}$$

whose diagonalization yields a set of triply ionized states

$$|\tilde{\Phi}_f^{N-3}\rangle = \sum_L c_{fL}|\Phi_L^{N-3}\rangle. \tag{10}$$

Different decay channels can be clearly identified among the $|\tilde{\Phi}_f^{N-3}\rangle$ states. A discretized representation of a scattering state corresponding to the open decay channel f is then obtained in the following

series of steps. First, a continuum electron is added to a virtual orbital p:

$$|\tilde{\Phi}^{N-2}_{p,f}\rangle = c^{\dagger}_{p}|\tilde{\Phi}^{N-3}_{f}\rangle. \tag{11}$$

Second, the $3h1p$ states $|\tilde{\Phi}^{N-2}_{p,f}\rangle$ are orthogonalized relative to the bound component $|\Phi_b\rangle$

$$|\bar{\Phi}^{N-2}_{p,f}\rangle = |\tilde{\Phi}^{N-2}_{p,f}\rangle - |\Phi_b\rangle\langle\tilde{\Phi}^{N-2}_{p,f}|\Phi_b\rangle, \tag{12}$$

yielding a set of states $|\bar{\Phi}^{N-2}_{p,f}\rangle$. Finally, the latter are further orthonormalized among themselves by a symmetric orthonormalization procedure:

$$|\bar{\Psi}^{N-2}_{p,f}\rangle = \sum_{p'}|\bar{\Phi}^{N-2}_{p',f}\rangle\left(\rho^{-\frac{1}{2}}\right)_{p'p} \tag{13}$$

$$\rho_{p',p} = \langle\bar{\Phi}^{N-2}_{p',f}|\bar{\Phi}^{N-2}_{p,f}\rangle. \tag{14}$$

The $3h1p$ states $|\bar{\Psi}^{N-2}_{p,f}\rangle$ are used to construct the projector onto the channel f:

$$\mathcal{P}_f = \sum_{p}|\bar{\Psi}^{N-2}_{p,f}\rangle\langle\bar{\Psi}^{N-2}_{p,f}|. \tag{15}$$

By construction the sum of partial widths, Γ_f, over the open channels should give, as required, the total width Γ. However, the errors involved in the numerical computation mean that the two quantities may differ. In the current calculation the sum over partial widths deviate from the total width by a factor of about 1.3. The final partial widths are, therefore, obtained by renormalization of the sum to the independently calculated total width.

The decay width calculations were performed using the cc-pVQZ basis sets on neon [36] and nonrelativistic cc-pVQZ [41] basis set on xenon. For an improved description of the pseudocontinuum additional $5s5p5d3f$ continuum like Kaufmann–Baumeister–Jungen (KBJ) [47] basis functions on neon, $7s7p7d4f1g$ basis functions on xenon and $2s2p1d$ midbond basis functions were used.

2.3. Nuclear dynamics and ETMD spectra

The nuclear dynamics accompanying the electronic decay process is described by using a theoretical framework based on the propagation of nuclear wave packets, described in detail in Ref. [13] to which the reader is referred. The nuclear wave packets propagating along the initial, decaying and final states PES are obtained by solving a system of coupled time-dependent Schrödinger equations. The Hamilton operator associated to each of the electronic states is given by the sum of the nuclear kinetic energy operator $\hat{T}_N$ and the associated potential energy operators $\hat{V}_i, \hat{V}_{d_j}$, and $\hat{V}_{f_k}$ obtained as described in Section 2.1, where i stays for initial, d for decaying and f for final state and the indices j and k number the decaying and final states, respectively. Additionally, for the decaying states the complex term $-i\Gamma^{d_j}/2$ has to be added, with Γ^{d_j} being the corresponding total decay width operator computed as in Section 2.2: this renders the Hamilton operator for the ETMD states non-hermitian. The partial decay width operator $\Gamma^{d_j}_{f_k}$ associated to the transition from a given decaying state to a specific final state f_k, is responsible instead for the coupling between the equations for the corresponding decaying and final wave packets. In principle, also the equations for the initial and the decaying wave packets are coupled through the excitation operator, which typically contains the transition dipole moment between the states. For the present study, however, the ionization process is assumed to be instantaneous, and the excitation operator independent on the nuclear coordinate. Furthermore, due to the much shorter Auger lifetime of the $Ne^{+}(1s^{-1})Xe$ state in comparison to the ETMD lifetime of the $Ne^{2+}(2p^{-2})Xe$ states, the nuclear dynamics is neglected also in the Auger decay step, so that the nuclear wave packet propagation is started by a vertical transition of the initial wave packet to the PES of the states decaying via ETMD, as done in similar dynamical studies of Auger-ICD cascades (see e.g. Refs. [18,48]). Therefore the initial condition is $\Psi_{d_j}(t_0) = \Psi_i(t_0)$, where Ψ_{d_j} is the wave packet propagating along the PES of thed^{th}_j decaying state and Ψ_i is the wave packet associated to the initial electronic state. The initial wave packet at time t_0, $\Psi_i(t_0)$, is taken to coincide with the lowest vibrational eigenstate of the electronic ground state of NeXe: it is therefore gaussian-like and centered at about 3.9 Å, the equilibrium distance of the ground state PES (see Section 3). The numerical grid used starts at 2 Å, ends at 11 Å and contains 1806 points, the wave packets are propagated for about 200 ps before convergence for all decay channels is obtained.

All the spectroscopic information required for the computation of the ETMD electron spectrum is contained in the wave packets for the final electronic states. In the absence of non-adiabatic couplings between the decaying and final states, the total electron spectrum is obtained as the sum of the partial spectra associated to the decay from each intermediate to each accessible final state, i.e.

$$\begin{aligned}\sigma^{fin}(E_{ETMD}) &= \lim_{t\to\infty}\sigma(E_{ETMD}, t)\\ &= \lim_{t\to\infty}\sum_j\sum_k\langle\psi^{d_j}_{f_k}(E_{ETMD}, t)|\psi^{d_j}_{f_k}(E_{ETMD}, t)\rangle,\end{aligned} \tag{16}$$

where E_{ETMD} is the energy of the emitted ETMD electron and $\psi^{d_j}_{f_k}(E_{ETMD})$ is the final wave packet propagating along the kth final state and resulting from the decay of the jth decaying state. Therefore, by the knowledge of the nuclear wave packets at each time, it is possible to follow the time evolution of the spectrum, given by $\sigma(E_{ETMD}, t)$.

The kinetic energy release spectrum for the fragments emitted after the decay is obtained from the electron decay spectrum by making use of the reflection principle [15], which is based on the principle of energy conservation and, therefore, exploits the relation $E_{TOT} = E_{ETMD} + E_{KER} + V^{\infty}_f$, where V^{∞}_f is the asymptotic value of the final state PES. Note however that, as it will become clear in Section 3, additional information about the different decay channels can be extracted from the KER, which is instead hidden in the electron spectrum.

3. Results and discussion

3.1. PECs of the initial and final states of ETMD

In this article we consider electron transfer mediated decay of doubly ionized states of NeXe populated by the Auger decay process of 1s-vacancy on Ne (see Eq. (1)). The Auger decay in weakly bound vander Waals clusters has overwhelmingly atomic character [49], therefore,the population of different Auger final states can be taken directly from the atomic data. In the case of Ne it is mostly different Ne^{2+} states (93%) which are produced with an insignificant admixture of the Ne^{3+} states (6%) [50]. Among the Ne^{2+} states the most populated are the ones characterized by the $2p^{-2}$ configuration: $Ne^{2+}(2p^{-2}\ ^1D)$ (61.2%) and $Ne^{2+}(2p^{-2}\ ^1S)$ (9.6%) [51]. These states lie at energies of 3.20 eV and 6.91 eV, respectively, above the ground state $Ne^{2+}(2p^{-2}\ ^3P)$; both excess energies are below the ionization potential of Xe (12.1 eV). However, attaching an electron to these states and producing $Ne^{+}(2p^{-1}\ ^2P)$ releases 44.2 eV and 47.9 eV, respectively, which is above the double ionization

potential of Xe (33.1 eV). Therefore, in NeXe these states will decay predominantly via ETMD, since ICD is energetically forbidden. Strong population of the $Ne^{2+}(2p^{-2})$ states in the Auger decay process and the absence of available electronic decay channels other than ETMD make these states ideal for the study of ETMD in rare gas dimers. The $Ne^{2+}(2s^{-1}2p^{-1}\,{}^1P)$ state which is also noticeably populated in the Auger decay (17.0%) undergoes ICD, whose signature is different from that of ETMD and can be recognized in a coincidence experiment [8,52]. Although the interatomic electronic decay channels are also open for the Ne^{3+} states, we will not study them in this article due to their low population.

The non-relativistic PECs of the doubly ionized states of NeXe which correlate with the decaying $Ne^{2+}(2p^{-2}\,{}^1D)Xe$ and $Ne^{2+}(2p^{-2}\,{}^1S)Xe$ are shown in Fig. 1. The five PECs of Σ, Π, and Δ symmetries which correspond to the former multiplet are virtually degenerate for all interatomic distances but the shortest. The PECs are bound and have the binding energies of 0.92–0.95 eV and the equilibrium distances ≈2.85 Å. The PEC of the $Ne^{2+}(2p^{-2}\,{}^1S)Xe$ (Σ) state has the binding energy of 0.95 eV at 2.90 Å. The minima of the PECs of both decaying states lie at shorter interatomic distances than the equilibrium distance R_0 = 3.90 Å in the electronic ground state of NeXe. Therefore, we expect ETMD to be accompanied by nuclear dynamics leading to the contraction of the average interatomic distance [30,31].

The non-relativistic final states of ETMD correlate at large interatomic distances with the $Ne^+(2p^{-1}\,{}^2P)Xe^{2+}(5p^{-2}\,{}^3P)$, $Ne^+(2p^{-1}\,{}^2P)Xe^{2+}(5p^{-2}\,{}^1D)$, and $Ne^+(2p^{-1}\,{}^2P)Xe^{2+}(5p^{-2}\,{}^1S)$ states. These states form three energetically well separated groups (see Fig. 1). Both $Ne^{2+}(2p^{-2}\,{}^1D)Xe$ and $Ne^{2+}(2p^{-2}\,{}^1S)Xe$ states decay into this manifold of states emitting an electron and setting off the Coulomb explosion of the Ne^+ and Xe^{2+} nuclei. Under the effect of the spin–orbit coupling the lowest group corresponding to the $Ne^+(2p^{-1}\,{}^2P)Xe^{2+}(5p^{-2}\,{}^3P)$ states will split into three corresponding to the three atomic terms of $Xe^{2+}(5p^{-2})$: ${}^3P_0$, ${}^3P_1$, and ${}^3P_2$ (see Fig. 2).

The manifold of the final states of ETMD is made complicated by the appearance of the states of $NeXe^{3+}(5p^{-3})$ character. Asymptotically these states lie only about 10 eV higher than the

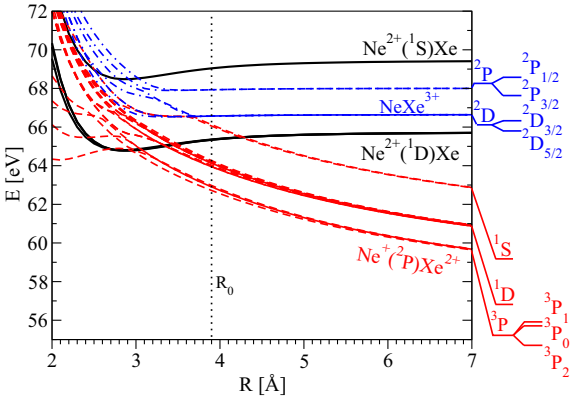

Fig. 1. Non-relativistic *ab initio* diabatic PECs of the decaying $Ne^{2+}(2p^{-2})Xe$ states and adiabatic PECs of the final Ne^+Xe^{2+} (dashed lines) and $NeXe^{3+}$ (dashed-dotted lines) states of ETMD. The PECs of the decaying states were shifted so as to match the experimental atomic energies as given in Ref. [53] at asymptotic separations. All final states were uniformly shifted so that the PECs of the $Ne^+(2p^{-1}\,{}^2P)Xe^{2+}(5p^{-2}\,{}^1D)$ match the asymptotic value available experimentally. The errors in the asymptotic energies of other states were <0.54 eV. Note, that ETMD of the $Ne^{2+}(2p^{-2}\,{}^1D)Xe$ leads only to the appearance of the Ne^+ and Xe^{2+} ions. The decay of the $Ne^{2+}(2p^{-2}\,{}^1S)Xe$ state can also produce the Ne, Xe^{3+} pair. The dotted vertical line denotes the equilibrium distance R_0 of the NeXe ground state.

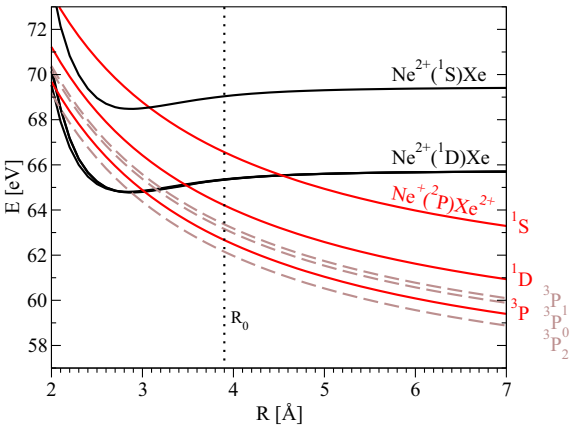

Fig. 2. (Solid lines) Non-relativistic diabatic PECs of the decaying $Ne^{2+}(2p^{-2})Xe$ states and the PECs of the final Ne^+Xe^{2+} states obtained using a phenomenological model. The final states are approximated by 2/R curves which have correct non-relativistic energies at the limit of the separated atoms. (Dashed lines) The 2/R curves corresponding to the spin–orbit split $Ne^+(2p^{-1}\,{}^2P)Xe^{2+}(5p^{-2}\,{}^3P)$ states. The dotted vertical line denotes the equilibrium distance R_0 of the NeXe ground state.

Ne^+Xe^{2+} states. Their PECs lie above the ones of the $Ne^{2+}(2p^{-2}\,{}^1D)Xe$ decaying state and are inaccessible from it in the electronic decay; however, the $Ne^{2+}(2p^{-2}\,{}^1S)Xe$ state can electronically decay into these states. Such decay may be termed double ETMD, since two electrons are transferred from Xe to Ne, while the third one is emitted into continuum. Double ETMD which involves three electrons of which two are transferred between atoms should be much slower than the normal ETMD which suggests that this channel might be neglected. However, the fast growing repulsive Ne^+Xe^{2+} states cross and interact with the $NeXe^{3+}$ states leading to the appearance of a series of avoided crossings between 2 Å and 4 Å, i.e. exactly at interatomic distances where ETMD takes place. Thus ETMD might efficiently proceed into a Ne^+Xe^{2+} state to be followed by the separation of the nuclei on an adiabatic PEC such that it is Ne and Xe^{3+} which are produced and not Ne^+ and Xe^{2+}.

This shows that if high precision is desired in the description of ETMD spectra of the $Ne^{2+}(2p^{-2}\,{}^1S)Xe$ state one needs the accurate knowledge of the positions of and coupling strengths at the avoided crossings between Ne^+Xe^{2+} and $NeXe^{3+}$ final states which can be obtained only in high level relativistic calculations. Moreover, to find accurate branching ratio of the decay into each of these two classes of final states calculation of the non-adiabatic nuclear dynamics in the final state is necessary. However, the decay of the $Ne^{2+}(2p^{-2}\,{}^1S)Xe$ state proceeds mostly into the Ne^+Xe^{2+} manifold; the decay to the $NeXe^{3+}$ states remains weak. Therefore, in our computations of the spectra we rely on a model Ne^+Xe^{2+} final state manifold introduced in the next paragraph, while the decay into $NeXe^{3+}$ states will be discussed qualitatively.

The PECs of the Ne^+Xe^{2+} final states behave very nearly as 2/R for the interatomic distances at which ETMD of the $Ne^{2+}(2p^{-2}\,{}^1D)Xe$ multiplet takes place. Therefore, we replace the respective PECs via the 2/R curves and shift the latter individually so that each matches the respective experimental energies at the separated atoms' limit (see Fig. 2). For the interatomic distances where ETMD into the respective final states is allowed the approximation works best for the PECs deriving from the $Ne^+(2p^{-1}\,{}^2P)Xe^{2+}(5p^{-2}\,{}^1S)$ states (cf. Figs. 1 and 2). The group of PECs corresponding to the $Ne^+(2p^{-1}\,{}^2P)Xe^{2+}(5p^{-2}\,{}^1D)$, which are degenerate at large interatomic distances, are not degenerate

anymore at the distances where the ETMD of $Ne^{2+}(2p^{-2}\ ^1D)Xe$ takes place. However, the energy splitting amounts to a few hundred meV atmost and will result in small changes of the spectra's shape. Finally, for the $Ne^{+}(2p^{-1}\ ^2P)Xe^{2+}(5p^{-2}\ ^3P)$ state a similar degeneracy lifting and the appearance of the avoided crossing with a $NeXe^{3+}$ state should similarly have a small impact on the ETMD spectra. The spin–orbit interaction in the $Ne^{+}(2p^{-1}\ ^2P)Xe^{2+}(5p^{-2}\ ^3P)$ multiplet is the most important relativistic effect in the final states manifold. Since the overall shape of the PECs will be mostly determined by the Coulomb repulsion between Ne^+ and Xe^{2+} in the range of R relevant for ETMD, the impact of this interaction will be to split the corresponding group of states into three. We can also use this model to estimate the ETMD spectra obtained in the decay of the $Ne^{2+}(2p^{-2}\ ^1S)Xe$ state, although the expected result will be less accurate due to the more complex structure of accessible final state manifold.

We can immediately use the phenomenological model of the ETMD final states in Fig. 2 for a qualitative discussion of the ETMD spectra. Thus, ETMD of the $Ne^{2+}(2p^{-2}\ ^1D)Xe$ state into the $Ne^{+}(2p^{-1}\ ^2P)Xe^{2+}(5p^{-2}\ ^1S)$ channel becomes forbidden at $R \gtrsim 4.5$ Å. Since the initial vibrational wavepacket is centered about $R_0 = 3.90$ Å, and the dynamics in the decaying state leads to the shortening of the average interatomic distance, the ETMD into this channel will be limited only to the exponential tail of the wavepacket and, thus, will be negligible. Therefore, ETMD proceeds mostly in the $Ne^{+}(2p^{-1}\ ^2P)Xe^{2+}(5p^{-2}\ ^1D)$ and $Ne^{+}(2p^{-1}\ ^2P)Xe^{2+}(5p^{-2}\ ^3P)$ channels which become closed at 3.45 Å and 3.00 Å, respectively. From the positions of the thresholds we conclude that the electron spectra cut-off lies at 0 eV, while the maximum KER available in the system is about 9.60 eV (10.10 eV if the spin–orbit splitting of the $Xe^{2+}(5p^{-2}\ ^3P)$ term is taken into account).

The decay from the $Ne^{2+}(2p^{-2}\ ^1S)Xe$ is possible into all three ETMD channels. Only the $Ne^{+}(2p^{-1}\ ^2P)Xe^{2+}(5p^{-2}\ ^1S)$ channel becomes closed at 3.05 Å, while the two other channels remain open for all interatomic distances of interest. Therefore, a large proportion of ETMD events will take place at the inner turning point $R_{in} \approx 2.45$ Å. The minimum electron energy expected in the decay of this state is, thus, about 0.55 eV, while the maximum KER is about 11.66 eV. The larger maximum KER in this case indicates that ETMD might take place at shorter interatomic distances compared to the case of the $Ne^{2+}(2p^{-2}\ ^1D)Xe$ state.

3.2. Total and partial ETMD widths

To obtain the full shape of the electron and KER spectra we first need to know the values of the total and partial ETMD widths for each decaying state. The total ETMD widths of the $^1\Sigma$, $^1\Pi$, and $^1\Delta$ terms which derive from the $Ne^{2+}(2p^{-2}\ ^1D)Xe$ multiplet are shown in Fig. 3. First we observe that for all but the shortest interatomic distances the widths show exponential behavior characteristic for the charge transfer driven processes. The sudden jumps at 4.55 Å, 3.45 Å, and 3.05 Å occur due to the closing of the $Ne^{+}(2p^{-1}\ ^2P)Xe^{2+}(5p^{-2}\ ^1S)$, $Ne^{+}(2p^{-1}\ ^2P)Xe^{2+}(5p^{-2}\ ^1D)$, and $Ne^{+}(2p^{-1}\ ^2P)Xe^{2+}(5p^{-2}\ ^3P)$ channels. The total widths of the $^1\Sigma$ and $^1\Pi$ terms are very similar for all R in question and are up to two orders of magnitude larger than the width of the $^1\Delta$ term. This ordering of the total decay widths can be explained by the different extent of the overlap between the hole density in Ne^{2+} and the valence electrons of Xe which determines the efficiency of the charge transfer. Thus the $^1\Sigma$ and $^1\Pi$ terms derive from the $p\sigma^{-2}$ and $p\sigma^{-1}p\pi^{-1}$ configurations

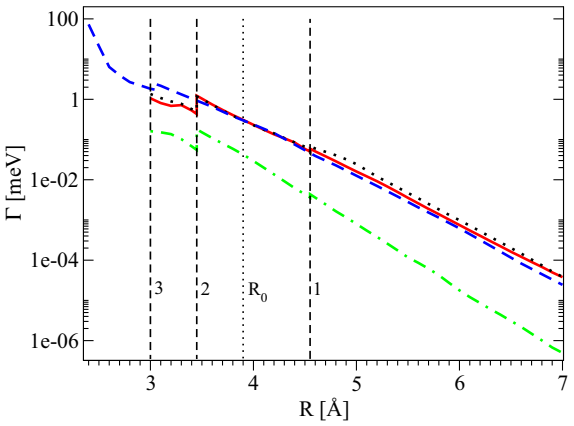

Fig. 3. Total ETMD widths of the terms deriving from the $Ne^{2+}(2p^{-2}\ ^1D)Xe$, and $Ne^{2+}(2p^{-2}\ ^1S)Xe$ decaying states. (Dashed line) $^1\Sigma$ term derived from the $Ne^{2+}(2p^{-2}\ ^1S)Xe$, (Dotted line) $^1\Sigma$ term, (Solid line) $^1\Pi$ term, (Dashed-dotted line) $^1\Delta$ term derived from the $Ne^{2+}(2p^{-2}\ ^1D)Xe$. The numbered dashed vertical lines enumerate different channel thresholds in the decay of the $Ne^{2+}(2p^{-2}\ ^1D)Xe$ multiplet: (1) $Ne^{+}(2p^{-1}\ ^2P)Xe^{2+}(5p^{-2}\ ^1S)$, (2) $Ne^{+}(2p^{-1}\ ^2P)Xe^{2+}(5p^{-2}\ ^1D)$, (3) $Ne^{+}(2p^{-1}\ ^2P)Xe^{2+}(5p^{-2}\ ^3P)$. The dotted vertical line denotes the equilibrium distance R_0 of the NeXe ground state.

of Ne^{2+} respectively. The hole in the $p\sigma$ orbital overlaps well with the valence electrons on Xe facilitating ETMD. On the contrary, the hole density in the $^1\Delta$ term is described by the $p\pi^{-2}$ configurations and overlaps much less with the electron density on Xe.

We next consider more closely the behavior of the total widths in the region where the dynamics during ETMD takes place. The total widths of the three terms at R_0 are 0.298 meV (2.18 ps), 0.308 meV (2.11 ps), and 0.042 meV (15.47 ps) for the $^1\Sigma$, $^1\Pi$, and $^1\Delta$ terms, respectively. The width grows with decreasing distance, however, it does so non-monotonically due to the closing of the $Ne^{+}(2p^{-1}\ ^2P)Xe^{2+}(5p^{-2}\ ^1D)$ channel at 3.45 Å. This behavior leads to an interesting result that for the $^1\Pi$, and $^1\Delta$ terms the width reaches maximum not at the shortest distance at which the decay is possible but at the $Ne^{+}(2p^{-1}\ ^2P)Xe^{2+}(5p^{-2}\ ^1D)$ threshold. For the $^1\Sigma$ term the values of the width at both thresholds (denoted (3) and (2) in Fig. 3) are very close. Therefore, due to the closing of the channels the total width oscillates in the range of R where the nuclear dynamics takes place during ETMD.

The behavior of the partial decay width will be discussed only briefly. Since our methods do not always allow the construction of channel projection operators, one often approximates the partial decay width by dividing the total width through the number of available final states. This approximation may lead to noticeable errors; however, their impact on the measurable spectra will be small if the final states are nearly degenerate and do not interact with other states. Therefore, in our case it is sufficient to compute only the partial decay widths into the groups of nearly degenerate states correlating with the $Ne^{+}(2p^{-1}\ ^2P)Xe^{2+}(5p^{-2}\ ^3P)$, $Ne^{+}(2p^{-1}\ ^2P)Xe^{2+}(5p^{-2}\ ^1D)$ and $Ne^{+}(2p^{-1}\ ^2P)Xe^{2+}(5p^{-2}\ ^1S)$ atomic multiplets. We could carry out such calculation of the partial widths only for the $Ne^{2+}(2p^{-2}\ ^1D)Xe$ decaying state. Interestingly, at $R \gtrsim 4.55$ Å where all three channels are open the ratio of partial widths is 3.3:4.0:1.0 (averaged over the initial $Ne^{2+}(2p^{-2}\ ^1D)Xe$ multiplet) which should be compared to the ratio of final states multiplicities 9:5:1. At R_0 where the decay into the $Ne^{+}(2p^{-1}\ ^2P)Xe^{2+}(5p^{-2}\ ^1S)$ is forbidden the ratio of the partial decay widths into the two remaining channels is 6:5 compared to the 9:5 ratio of their multiplicities.

The behavior of the total ETMD width of the $^1\Sigma$ term deriving from the $Ne^{2+}(2p^{-2}\ ^1S)Xe$ state is also shown in Fig. 3. An impor-

tant difference between the Γ of this state and the states considered previously is that ETMD channels remain open for all R's where the nuclear dynamics during ETMD takes place. This state is dominated by the $p\sigma^{-2} + p\pi^{-2}$ configuration and, therefore, at larger R exhibits similar overlap between Ne^{2+} and Xe and the total decay width similar to ones of the $^1\Sigma, ^1\Pi$ terms of the $Ne^{2+}(2p^{-2}\ ^1D)Xe$ state. Up to the threshold at 3.05 Å the width behaves nearly exponential, while at shorter distances it is strongly enhanced due to the admixture of states of the $Ne^{+}(2p-1)Xe^{+}(5s^{-1})$ character. At R_0 the total width is 0.30 meV (2.17 ps), however, at R = 2.4 Å the combined effect of the shorter interatomic distance and the electron delocalization between Xe and Ne^{2+} leads to the ETMD width of 72.91 meV (8.92 fs). To compute the partial widths in the decay of the $Ne^{2+}(2p^{-2}\ ^1S)Xe$ state we had to resort to dividing the total ETMD width through the weights of the final states multiplets. As we discuss in the Methods the definition of the channel projectors becomes difficult due to the mixing of the $Ne^{+}Xe^{2+}$ and $NeXe^{3+}$ states. The computed partial widths ratios in the case of the $Ne^{2+}(2p^{-2}\ ^1D)Xe$ multiplet allow us to estimate the errors incurred.

3.3. ETMD electron and KER spectra

Using the ETMD widths in Fig. 3 and the non-relativistic phenomenological PECs shown in Fig. 2 we computed ETMD electron and KER spectra plotted in Figs. 4 and 5, respectively. We also estimated the effect of the spin–orbit splitting on the spectra and found it to be limited as discussed in the last paragraphs of this section. The easiest to interpret are the spectra of the $Ne^{2+}(2p^{-2}\ ^1S)Xe$ state.The KER spectrum (see Fig. 5(a)), which shows what is the probability for the decay to take place at aspecific R, appears as a single narrow peak at 12 eV indicating that ETMD occurs predominantly at the inner turning point of the decaying state PEC at 2.45 Å. ETMD proceeds almost exclusively into the $Ne^{+}(2p^{-1}\ ^2P)Xe^{2+}(5p^{-2}\ ^1D)$ and $Ne^{+}(2p^{-1}\ ^2P)Xe^{2+}(5p^{-2}\ ^3P)$ channels which are open for all R of interest, while the decay into the $Ne^{+}(2p^{-1}\ ^2P)Xe^{2+}(5p^{-2}\ ^1S)$ channel is negligible.

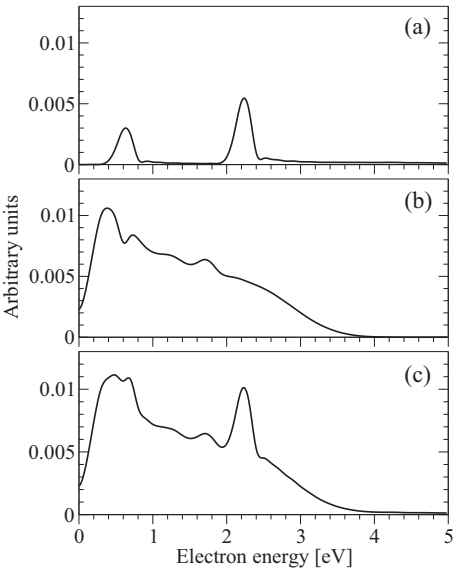

Fig. 4. ETMD electron spectra computed using the final state manifold in Fig. 2. (a) Electron spectrum corresponding to the decay of the $Ne^{2+}(2p^{-2}\ ^1S)Xe$ state. (b) Electron spectrum corresponding to the decay of the $Ne^{2+}(2p^{-2}\ ^1D)Xe$ state. (c) Total electron spectrum obtained by summing the spectra in (a) and (b). The ratio of the integrated spectra in panels (a) and (b) corresponds to the ratio of the respective populations (1:6) of the ETMD decaying states reached in the Auger decay.

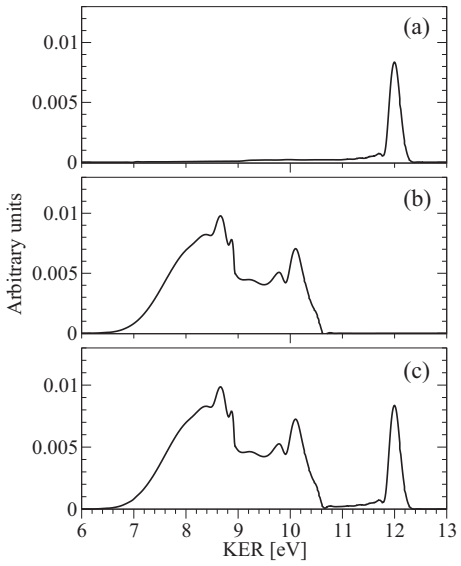

Fig. 5. KER spectra computed using the final state manifold in Fig. 2. (a) KER spectrum corresponding to the decay of the $Ne^{2+}(2p^{-2}\ ^1S)Xe$ state. (b) KER spectrum corresponding to the decay of the $Ne^{2+}(2p^{-2}\ ^1D)Xe$ state. (c) Total KER spectrum obtained by summing the spectra in (a) and (b). The ratio of the integrated spectra in panels (a) and (b) corresponds to the ratio of the respective populations (1:6) of the ETMD decaying states reached in the Auger decay.

The decay into these two energetically separated channels is well visible in the ETMD electron spectrum (see Fig. 4(a)) as two sharp peaks at 0.7 eV and 2.2 eV. The narrow width of the peaks in both electron and KER spectra is due to the behavior of the total ETMD width which grows almost ten-fold between the minimum of the decaying state's PEC and the inner turning point.

The electron spectrum due to ETMD of the $Ne^{2+}(2p^{-2}\ ^1D)Xe$ state (see Fig. 4(b)) appears as one broad peak between 0 eV and 4 eV. The overwhelming contribution to this peak comes again from the decay into the $Ne^{+}(2p^{-1}\ ^2P)Xe^{2+}(5p^{-2}\ ^1D)$ and $Ne^{+}(2p^{-1}\ ^2P)Xe^{2+}(5p^{-2}\ ^3P)$ channels which close at distances smaller than R_0. The appearance of this spectrum which is so different from the spectra of the $Ne^{2+}(2p^{-2}\ ^1S)Xe$ state is due to the fact that none of the ETMD channels remains open for all R where nuclear dynamics take place. It leads to the behavior of the total width which we noted above - instead of reaching a maximum at the smallest available R it exhibits two maxima, one at each threshold. Since the probability of the decay does not vary much in the interval of R where the nuclei move, it results in a broad distribution of the energies of the emitted electrons. Another consequence of this behavior of Γ is the appearance of the vibrational structure in the spectrum with the peaks at 0.4 eV and 1.9 eV corresponding to the decay close to the ETMD thresholds. Our calculations show that this structure is due to the decay into the $Ne^{+}(2p^{-1}\ ^2P)Xe^{2+}(5p^{-2}\ ^3P)$ channel (see Fig. 6).

The KER spectrum due to the ETMD of the $Ne^{2+}(2p^{-2}\ ^1D)Xe$ state lies between 6.5 and 10.5 eV (see Fig. 5(b)) and is also quite structured. The peaks at approximately 8.5 and 10 eV correspond to the thresholds of the $Ne^{+}(2p^{-1}\ ^2P)Xe^{2+}(5p^{-2}\ ^1D)$ and $Ne^{+}(2p^{-1}\ ^2P)Xe^{2+}(5p^{-2}\ ^3P)$ channels respectively. We see prominent peaks marking the channel thresholds due to the non-monotonic behavior of the total ETMD width which has maxima at the respective R. Moreover, these peaks are distinguishable in the KER spectra, since the thresholds lie at different values of the interatomic distance. Again a vibrational structure is visible in the spectrum due to the decay to the $Ne^{+}(2p^{-1}\ ^2P)Xe^{2+}(5p^{-2}\ ^3P)$ state.

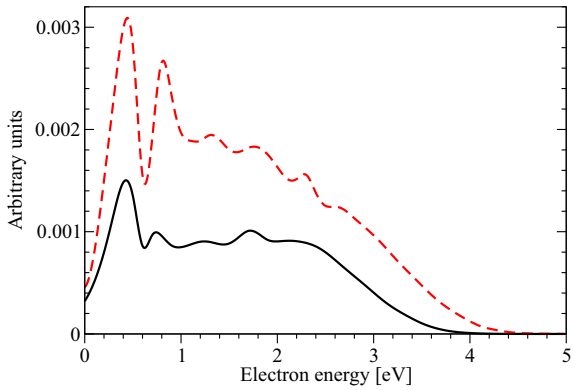

Fig. 6. Comparison of the electron spectra obtained in ETMD of the $Ne^{2+}(2p^{-2}\ ^1D)Xe\ ^1\Sigma$ term into the $Ne^{+}(2p^{-1}\ ^2P)Xe^{2+}(5p^{-2}\ ^3P)$ channel with (dashed line) and without (solid line) taking into account the spin–orbit splitting of the $Xe^{2+}(5p^{-2}\ ^3P)$ multiplet. Note the vibrational structure visible in both spectra. Similar vibrational structure appearing in the ETMD spectra of the $Ne^{2+}(2p^{-2}\ ^1D)Xe$ state (see Figs. 4(b) and 5(b)) is due to the decay into the $Ne^{+}(2p^{-1}\ ^2P)Xe^{2+}(5p^{-2}\ ^3P)$ channel.

Adding up the ETMD spectra of the $Ne^{2+}(2p^{-2}\ ^1D)Xe$ and $Ne^{2+}(2p^{-2}\ ^1S)Xe$ states we obtain the total ETMD electron (Fig. 4(c)) and KER (Fig. 5(c)) spectra which should be observable in NeXe following the Auger decay of the 1s-vacancy on Ne. One may immediately see that the two electron spectra overlap making it difficult to discern the contributions of ETMD from the different decaying states. The KER spectra, on the contrary, are well separated energetically with the sharp peak due to the ETMD of the $Ne^{2+}(2p^{-2}\ ^1S)Xe$ state clearly visible at 12 eV. This spectral structure offers a convenient opportunity to investigate the ETMD of the two decaying states independently. Thus, a measurement of slow electrons coincident with the Ne^+ and Xe^{2+} nuclei which have 12 eV of KER should give the electron spectrum in Fig. 4(a). The electron spectrum corresponding to the ETMD of $Ne^{2+}(2p^{-2}\ ^1D)Xe$ can be obtained by collecting slow electrons coincident with the nuclei having 6–10.5 eV of KER.

We would also like to note that the PECs of Σ and Π symmetries corresponding to the lower lying $Ne^{2+}(2p^{-2}\ ^1D)Xe$ state cross at about 3.5 Å the respective PECs of the $Ne^{+}(2s^{-1}\ ^2S)Xe(5p^{-1}\ ^2P)$ state which is not populated directly in the Auger decay. Therefore, nuclear dynamics which is set off by the Auger decay may lead to the electron transfer and population of the $Ne^{+}(2s^{-1}\ ^2S)Xe(5p^{-1}\ ^2P)$ state. The latter is electronically unstable and decays by ICD into the same final states as ETMD. In addition to ICD, populating the $Ne^{+}(2s^{-1}\ ^2S)Xe(5p^{-1}\ ^2P)$ state leads to the Coulomb explosion of the cluster. Since ICD rate decreases fast with the interatomic distance the majority of ICD events will take place close to the crossing point resulting in the electrons of 0–1.6 eV and KER of about 8.2 eV. These values lie within the ETMD electron and KER spectra. Although the energy splitting due to the crossing was found to be 0.04–0.1 eV we assume the non-adiabatic coupling to be weak, since electron transfer is accompanied by the excitation of a 2s-electron of Ne. Therefore, we do not expect that the signal from this sequential electron transfer ICD process will be discernible in the experimental spectra.

To estimate the effect that the spin–orbit splitting of the $Ne^{+}(2p^{-1}\ ^2P)Xe^{2+}(5p^{-2}\ ^3P)$ final state would have on the ETMD spectra of the $Ne^{2+}(2p^{-2}\ ^1D)Xe$ state we computed the electron spectra for the decay of the $Ne^{2+}(2p^{-2}\ ^1D)Xe\ ^1\Sigma$ state using the model curves for the split $Xe^{2+}(5p^{-2}\ ^3P)$ multiplet. The results shown in Fig. 6 indicate that the overall appearance of the spectrum remains very much the same. However, the integrated intensity of the spectrum in the spin- orbit case is larger indicating that the decay into the $Ne^{+}(2p^{-1}\ ^2P)Xe^{2+}(5p^{-2}\ ^3P)$ becomes more probable. This is due to the shifting of the ETMD thresholds so that the contribution of the $^3P_2$ channel which closes at shorter interatomic distances outweighs the contributions of the $^3P_0$ and $^3P_1$ channels which close at longer ones. We expect the effect of the spin–orbit splitting on the spectra of the $^1\Pi$ and $^1\Delta$ terms to be similar. Importantly, the spin–orbit splitting of the final state does not destroy the vibrational structure visible in the spectra.

In the case of the $Ne^{2+}(2p^{-2}\ ^1S)Xe$ state the spin–orbit splitting will have no effect on the KER spectrum, since the latter is defined by the value of R at which the decay predominantly takes place. However, in the corresponding electron spectrum the peak at 2.2 eV will be split into three reflecting the splitting of the $Ne^{+}(2p^{-1}\ ^2P)Xe^{2+}(5p^{-2}\ ^3P)$ multiplet in the final state.

We would like to conclude the discussion of the results by some qualitative consideration of ETMD into the $NeXe^{3+}$ channel possible from the $Ne^{2+}(2p^{-2}\ ^1S)Xe$ state. Decay onto the PECs denoted by the dashed-dotted lines in Fig. 1 will lead to the dissociation of the dimer and the production of Ne and Xe^{3+} if the adiabatic nuclear dynamics takes place on the final PEC. Assuming that the decay is the strongest at the thresholds or the inner turning point of the decaying PEC we can estimate that the ETMD electrons will have energy between 0 eV and 1 eV. The KER of Ne and Xe^{3+} lies between 1.5 eV and 3 eV. Therefore, the corresponding decay should be seen from the coincidence of an electron with energy <1 eV with the Xe^{3+} having energy between 0.2 eV and 0.4 eV. Due to the relatively low population of the $Ne^{2+}(2p^{-2}\ ^1S)Xe$ state and a small number of accessible $NeXe^{3+}$ states the probability of such coincident events may not be large. However, experimental observation of such events will be an important demonstration of the impact that nuclear dynamics in the final states have on the ETMD process.

4. Conclusions

In this work we carried out an *ab initio* study of electron transfer mediated decay (ETMD) of $Ne^{2+}(2p^{-2})Xe$ states abundantly produced in NeXe dimer following the normal Auger decay of a 1s-vacancy on Ne. Our calculations show that the states deriving from the $Ne^{2+}(2p^{-2}\ ^1D)Xe$ and $Ne^{2+}(2p^{-2}\ ^1S)Xe$ multiplets efficiently decay into the $Ne^{+}(2p^{-1}\ ^2P)Xe^{2+}(5p^{-2}\ ^3P)$, $Ne^{+}(2p^{-1}\ ^2P)Xe^{2+}(5p^{-2}\ ^1D)$, and $Ne^{+}(2p^{-1}\ ^2P)Xe^{2+}(5p^{-2}\ ^1S)$ ETMD final states. The decay is accompanied by the emission of a slow electron and the Coulomb explosion of Ne^+ and Xe^{2+}. We found that ETMD channels remain open for the $Ne^{2+}(2p^{-2}\ ^1S)Xe$ state for the interatomic distances, R, at which nuclear dynamics take place in the decaying state. In the case of the $Ne^{2+}(2p^{-2}\ ^1D)Xe$ multiplet they become closed one by one in the relevant range of R. Thus the ETMD electron and KER spectra of the two multiplets have completely different shape.

In the case of the $Ne^{2+}(2p^{-2}\ ^1S)Xe$ state the decay happens at a narrow range of R close to the inner turning point in the respective PEC. This is due to the strong exponential growth of the ETMD width with decreasing R, so that the ETMD lifetime becomes as short as 9 fs at the turning point compared with the 2.2 ps at the electronic ground state equilibrium distance. This leads to the KER spectrum consisting of a single narrow peak at 12 eV. The electron spectrum comprises two narrow peaks at 0.7 eV and 2.2 eV corresponding to the decay into two open and energetically separated channels: $Ne^{+}(2p^{-1}\ ^2P)Xe^{2+}(5p^{-2}\ ^3P)$ and $Ne^{+}(2p^{-1}\ ^2P)Xe^{2+}(5p^{-2}\ ^1D)$.

The spectra due to the decay of the $Ne^{2+}(2p^{-2}\ ^1D)Xe$ has a completely different appearance. Although the decay still

predominantly proceeds into the $Ne^{+}(2p^{-1}\ ^{2}P)Xe^{2+}(5p^{-2}\ ^{1}D)$ and $Ne^{+}(2p^{-1}\ ^{2}P)Xe^{2+}(5p^{-2}\ ^{3}P)$ channels both become closed in the range of R where the nuclear dynamics take place. This leads to a non-monotonic behavior of the ETMD width so that it does not strongly vary in this range. This results in broad peaks in the electron (0–4 eV) and KER (6.5–10.5 eV) spectra which exhibit vibrational structure. Since the total ETMD width has maxima at the positions of the thresholds, the latter become visible both in the electron and KER spectra.

The clear separation between the KER peaks offers a way to observe the decay from the $Ne^{2+}(2p^{-2}\ ^{1}D)Xe$ and $Ne^{2+}(2p^{-2}\ ^{1}S)Xe$ states separately. Measuring slow electrons in coincidence with the Ne^{+} and Xe^{2+} ions having about 12 eV KER should reproduce the electron spectra of the $Ne^{2+}(2p^{-2}\ ^{1}S)Xe$ state. A similar measurement of these ions with KER between 6.5 eV and 10.5 eV should give the $Ne^{2+}(2p^{-2}\ ^{1}D)Xe$ electron spectrum.

At last, we observed that the PECs of the $Ne^{+}Xe^{2+}$ states may cross and interact with the PECs of the $NeXe^{3+}$ states in the range of interatomic distances where ETMD occurs. From the energetic considerations only the $Ne^{2+}(2p^{-2}\ ^{1}S)Xe$ state can decay into the $NeXe^{3+}$ manifold. Such decay entails the transfer of two electrons, while a third is emitted into the electronic continuum which should make this process much slower than the normal ETMD. However, the decay into such states might occur in directly following the normal ETMD into a $Ne^{+}Xe^{2+}$ state which interacts with the $NeXe^{3+}$ one. The subsequent nuclear dynamics on an adiabatic final PEC will lead to the dissociation of the dimer which produces Ne and Xe^{3+}. We estimated that a possible signature of such process would be a coincident observation of electrons with energies <1 eV and Xe^{3+} nuclei with energies 0.2–0.4 eV. This shows that in properly accounting for the products of ETMD non-adiabatic nuclear dynamics in the final states is important. Moreover,since triple ionization potentials in larger molecules may not be that far away from the double ionization potentials similar effects would be very important whenever ETMD takes place between a multiply charged ion and such a molecule.

Acknowledgements

The authors wish to dedicate this article to Lorenz Cederbaum, a friend and a teacher, on occasion of his 70-th birthday. S.S. thanks the Brigitte–Schlieben–Lange program of ministry of science and culture of Baden-Württemberg for financial support. Financial support of the Deutsche Forschungsgemeinschaft (DFG research unit 1789) is gratefully acknowledged.

References

[1] W. Bambynek, B. Crasemann, R.W. Fink, H.U. Freund, H. Mark, C.D. Swift, R.E. Price, P.V. Rao, Rev. Mod. Phys. 44 (1972) 716.
[2] L.S. Cederbaum, J. Zobeley, F. Tarantelli, Phys. Rev. Lett. 79 (1997) 4778.
[3] T. Jahnke, J. Phys. B 48 (2015) 082001.
[4] M. Förstel, T. Arion, U. Hergenhahn, J. Electron. Spectrosc. Relat. Phenom. 191 (2013) 16.
[5] S. Kopelke, Y.C. Chiang, K. Gokhberg, L.S. Cederbaum, J. Chem. Phys. 137 (2012) 034302.
[6] G. Jabbari, K. Sadri, L.S. Cederbaum, K. Gokhberg, J. Chem. Phys. 144 (2016) 164307.
[7] R. Santra, L.S. Cederbaum, Phys. Rev. Lett. 90 (2003) 153401.
[8] Y. Morishita, X.-J. Liu, N. Saito, T. Lischke, M. Kato, G. Prümper, M. Oura, H. Yamaoka, Y. Tamenori, I.H. Suzuki, K. Ueda, Phys. Rev. Lett. 96 (2006) 243402.
[9] K. Gokhberg, P. Kolorenč, A.I. Kuleff, L.S. Cederbaum, Nature 505 (2014) 661.
[10] F. Trinter, M.S. Schöffler, H.K. Kim, F.P. Sturm, K. Cole, N. Neumann, A. Vredenborg, J. Williams, I. Bocharova, R. Guillemin, M. Simon, A. Belkacem, A.L. Landers, T. Weber, H. Schmidt-Böcking, R. Dörner, T. Jahnke, Nature 505 (2014) 664.
[11] E. Alizadeh, T.M. Orlando, L. Sanche, Annu. Rev. Phys. Chem. 66 (2015) 379.
[12] R. Santra, J. Zobeley, L.S. Cederbaum, N. Moiseyev, Phys. Rev. Lett. 85 (2000) 4490.
[13] S. Scheit, L.S. Cederbaum, H.-D. Meyer, J. Chem. Phys. 118 (2003) 2092.
[14] T. Jahnke, A. Czasch, M.S. Schöffler, S. Schlössler, A. Knapp, M. Käsz, J. Titze, C. Wimmer, K. Kreidi, R.E. Grisenti, A. Staudte, O. Jagutzki, U. Hergenhahn, H. Schmidt-Böcking, R. Dörner, Phys. Rev. Lett. 93 (2004) 163401.
[15] S. Scheit, V. Averbukh, H.-D. Meyer, N. Moiseyev, R. Santra, T. Sommerfeld, J. Zobeley, L.S. Cederbaum, J. Chem. Phys. 121 (2004) 8393.
[16] K. Kimura, H. Fukuzawa, T. Tachibana, Y. Ito, S. Mondal, M. Okunishi, M. Schöffler, J. Williams, Y. Jiang, Y. Tamenori, N. Saito, K. Ueda, J. Phys. Chem. Lett. 4 (2013) 1838.
[17] P. O'Keeffe, E. Ripani, P. Bolognesi, M. Coreno, M. Devetta, C. Callegari, M. Di Fraia, K.C. Prince, R. Richter, M. Alagia, A. Kivimäki, L. Avaldi, J. Phys. Chem. Lett. 4 (2013) 1797.
[18] T. Miteva, Y.-C. Chiang, P. Kolorenč, A.I. Kuleff, K. Gokhberg, L.S. Cederbaum, J. Chem. Phys. 141 (2014) 064307.
[19] N. Sisourat, N.V. Kryzhevoi, P. Kolorenč, S. Scheit, T. Jahnke, L.S. Cederbaum, Nat. Phys. 6 (2010) 508.
[20] K. Schnorr, A. Senftleben, M. Kurka, A. Rudenko, L. Foucar, G. Schmid, A. Broska, T. Pfeifer, K. Meyer, D. Anielski, R. Boll, D. Rolles, M. Kübel, M.F. Kling, Y.H. Jiang, S. Mondal, T. Tachibana, K. Ueda, T. Marchenko, M. Simon, G. Brenner, R. Treusch, S. Scheit, V. Averbukh, J. Ullrich, C.D. Schröter, R. Moshammer, Phys. Rev. Lett. 111 (2013) 093402.
[21] F. Trinter, J.B. Williams, M. Weller, M. Waitz, M. Pitzer, J. Voigtsberger, C. Schober, G. Kastirke, C. Müller, C. Goihl, P. Burzynski, F. Wiegandt, T. Bauer, R. Wallauer, H. Sann, A. Kalinin, L. Schmidt, M. Schöffler, N. Sisourat, T. Jahnke, Phys. Rev. Lett. 111 (2013) 093401.
[22] J. Zobeley, R. Santra, L.S. Cederbaum, J. Chem. Phys. 115 (2001) 5076.
[23] V. Averbukh, L.S. Cederbaum, J. Chem. Phys. 123 (2005) 204107.
[24] M. Pernpointner, N.V. Kryzhevoi, S. Urbaczek, J. Chem. Phys. 129 (2008) 024304.
[25] J.P. Zobel, N.V. Kryzhevoi, M. Pernpointner, J. Chem. Phys. 140 (2014) 161103.
[26] E. Faßhauer, N.V. Kryzhevoi, M. Pernpointner, J. Chem. Phys. 133 (2010) 014303.
[27] E. Faßhauer, M. Pernpointner, K. Gokhberg, J. Chem. Phys. 138 (2013) 014305.
[28] M. Förstel, M. Mucke, T. Arion, A.M. Bradshaw, U. Hergenhahn, Phys. Rev. Lett. 106 (2011) 033402.
[29] K. Sakai, S. Stoychev, T. Ouchi, I. Higuchi, M. Schöffler, T. Mazza, H. Fukuzawa, K. Nagaya, M. Yao, Y. Tamenori, A.I. Kuleff, N. Saito, K. Ueda, Phys. Rev. Lett. 106 (2011) 033401.
[30] V. Stumpf, P. Kolorenč, K. Gokhberg, L.S. Cederbaum, Phys. Rev. Lett. 110 (2013) 258302.
[31] V. Stumpf, N.V. Kryzhevoi, K. Gokhberg, L.S. Cederbaum, Phys. Rev. Lett. 112 (2014) 193001.
[32] V. Stumpf, K. Gokhberg, L.S. Cederbaum, Nat. Chem. 8 (2016) 237.
[33] A.C. LaForge, V. Stumpf, K. Gokhberg, J. von Vangerow, F. Stienkemeier, N.V. Kryzhevoi, P. O'Keeffe, A. Ciavardini, S.R. Krishnan, M. Coreno, K.C. Prince, R. Richter, R. Moshammer, T. Pfeifer, L.S. Cederbaum, M. Mudrich, Phys. Rev. Lett. 116 (2016) 203001.
[34] We disregard radioactively unstable NeRn.
[35] M.W. Schmidt, K.K. Baldridge, J.A. Boatz, S.T. Elbert, M.S. Gordon, J.H. Jensen, S. Koseki, N. Matsunaga, K.A. Nguyen, S. Su, T.L. Windus, M. Dupuis, J.A. Montgomery, J. Comput. Chem. 14 (1993) 1347.
[36] K.L. Schuchardt, B.T. Didier, T. Elsethagen, L. Sun, V. Gurumoorthi, J. Chase, J. Li, T.L. Windus, Basis set exchange: a community database for computational sciences, J. Chem. Inf. Model. 47 (3) (2007) 1045.
[37] F.-M. Tao, Y.-K. Pan, J. Chem. Phys. 97 (1992) 4989.
[38] J. Schirmer, A. Barth, Z. Phys. A 317 (1984) 267.
[39] F. Tarantelli, L.S. Cederbaum, Phys. Rev. A 46 (1992) 81.
[40] G. Karlström, R. Lindh, P.-A. Malmqvist, B.O. Roos, U. Ryde, V. Veryazov, P.-O. Widmark, M. Cossi, B. Schimmelpfennig, P. Neogrady, L. Seijo, Comp. Mater. Sci. 28 (2003) 222.
[41] A. Mahler, A.K. Wilson, J. Chem. Phys. 142 (2015) 084102.
[42] P. Kolorenč, V. Averbukh, K. Gokhberg, L.S. Cederbaum, J. Chem. Phys. 129 (2008) 244102.
[43] P. Kolorenč, N. Sisourat, J. Chem. Phys. 143 (2015) 224310.
[44] U. Fano, Phys. Rev. 124 (1961) 1866.
[45] F. Mertins, J. Schirmer, Phys. Rev. A 53 (1996) 2140.
[46] F. Müller-Plathe, G. Diercksen, Phys. Rev. A 40 (1989) 696.
[47] K. Kaufmann, W. Baumeister, M. Jungen, J. Phys. B 22 (1989) 2223.
[48] P.V. Demekhin, S. Scheit, S.D. Stoychev, L.S. Cederbaum, Phys. Rev. A 78 (2008) 043421.
[49] K. Kimura, H. Fukuzawa, K. Sakai, S. Mondal, E. Kukk, Y. Kono, S. Nagaoka, Y. Tamenori, N. Saito, K. Ueda, Phys. Rev. A 87 (2013) 043414.
[50] B. Kanngieer, M. Jainz, S. Brünken, W. Benten, C. Gerth, K. Godehusen, K. Tiedtke, P. van Kampen, A. Tutay, P. Zimmermann, V.F. Demekhin, A.G. Kochur, Phys. Rev. A 62 (2000) 014702.
[51] H.P. Kelly, Phys. Rev. A 11 (1975) 556.
[52] T. Ouchi, K. Sakai, H. Fukuzawa, I. Higuchi, P.V. Demekhin, Y.-C. Chiang, S.D. Stoychev, A.I. Kuleff, T. Mazza, M. Schöffler, K. Nagaya, M. Yao, Y. Tamenori, N. Saito, K. Ueda, Phys. Rev. A 83 (2011) 053415.
[53] A.E. Kramida, Y. Ralchenko, J. Reader, NIST ASD TEAM, NIST Atomic Spectra Database (version 5.3), [Online]. Available: http://physics.nist.gov/asd. National Institute of Standards and Technology, Gaithersburg, MD, 2015.